

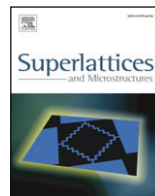


ELSEVIER

Contents lists available at ScienceDirect

Superlattices and Microstructures

journal homepage: www.elsevier.com/locate/superlattices



CL study of yellow emission in ZnO nanostructures annealed in Ar and O₂ atmospheres

A. González^a, M. Herrera-Zaldívar^{b,*}, J. Valenzuela^b, A. Escobedo-Morales^c, U. Pal^c

^a Centro de Investigación Científica y de Educación Superior de Ensenada, Apartado Postal 2732, Ensenada, Baja California 22860, Mexico

^b Centro de Nanociencias y Nanotecnología, Universidad Nacional Autónoma de México, Apdo. Postal 356, Ensenada, BC 22800, Mexico

^c Instituto de Física, Universidad Autónoma de Puebla, Apdo. Postal J-48, Puebla, Pue. 72570, Mexico

ARTICLE INFO

Article history:

Available online 11 December 2008

Keywords:

ZnO

Cathodoluminescence

Point defects

Indium doping

ABSTRACT

The yellow emission of thermally treated undoped and In doped ZnO nanostructures was studied by the cathodoluminescence (CL) technique. CL spectra acquired at room temperature of the as-grown samples revealed two emissions at about 3.2 eV and 2.13 eV, corresponding to the near band edge and defect related emissions, respectively. On annealing the samples at 600 °C in Ar and O₂ atmospheres, the defect emission suffers a red shift, irrespective of the annealing atmosphere. This red shift is explained in terms of variations in the relative intensities of the two component bands centered at about 2.24 eV and 1.77 eV, which were clearly resolved in the CL spectra acquired at low temperature of the annealed samples. A decrease of the relative intensity of the yellow emission (2.24 eV) was observed for all thermally annealed samples. The annealing of zinc interstitial point defects is proposed as a possible mechanism to explain this intensity decrease.

© 2008 Elsevier Ltd. All rights reserved.

1. Introduction

Luminescence properties of ZnO nanostructures have been extensively studied in the last few years due to their potential applications in the fabrication of highly efficient blue lasers and light-emitting

* Corresponding address: CNYN-UNAM, P.O. Box 439036, San Ysidro, 92143-CA, USA. Tel.: +52 646 174 4602; fax: +52 646 174 4603.

E-mail address: zaldivar@cnyunam.mx (M. Herrera-Zaldívar).

diodes [1,2], gas sensors [3,4] and photocatalysts [5]. While the large exciton binding energy of ZnO (60 meV) facilitates the gain mechanism in such devices, an increase in the number of shallow states by adequate doping can decrease its excitation energy with better electronic transport. Therefore, a great effort is being devoted in doping ZnO nanostructures by several impurities like In, Ga, and Sb [6–9]. Incorporation of impurities in semiconductors, however, regularly produces crystalline defects that generate undesired luminescence in their radiative spectra.

Different luminescent techniques have been used to characterize the optical properties of defects in semiconductors, with enough sensitivity even for low concentrations of such defects [10–12]. In particular, cathodoluminescence (CL) in the scanning electron microscope (SEM) has been applied to study the spectral and spatial distribution of defect emissions in ZnO nanostructures [13,14]. These reports indicate that in addition to their morphology, growth orientation and preparation methods, the defects strongly influence the luminescent behaviour of ZnO nanostructures. The most common defect related emission in ZnO is the broad green–yellow luminescence centered about of 2.2 eV, which has been widely attributed to native point defects like oxygen vacancies [15] and intrinsic or complex defects [16]. Recently we reported the presence of defect states at 2.2 eV above the valence band in ZnO nanorods grown by the hydrothermal method, and attributed them to point defects formed by a surface strain relaxation process [17].

Understanding the nature of crystal defects together with their spatial distribution and their effects on the luminescent properties of the ZnO would enable us to get insight onto the emission mechanisms in nanostructures. In order to investigate the effects of crystal defects on the luminescent properties of undoped and In doped ZnO nanostructures, CL microscopy and spectroscopy were used in this work.

2. Experimental

Undoped and In doped ZnO nanostructured samples were grown by a low-temperature hydrothermal process following the procedure reported earlier [18]. Briefly, ethylenediamine, zinc acetate, and sodium hydroxide were used as reactives in the synthesis process at 90 °C. For doping, the desired amount of indium chloride (nominally 0.5, 1.0 and 2.0 mol%) was added to the reaction mixture. Under our experimental conditions, indium doping of ZnO through the hydrothermal process resulted in the formation of an indium hydroxide phase, which could be dissociated and partially incorporated into the ZnO nanostructures in elemental form through subsequent annealing at 300 °C in an argon atmosphere for 2 h.

The obtained powder samples were attached to a copper sample holder for EDS and CL analysis in a Jeol JSM 5300 SEM microscope, with a typical electron beam energy of 15 KeV. CL measurements were performed at sample temperatures between 100 K and 300 K in the UV–visible spectral range using a monochromator and a photomultiplier detector for spectral analysis. Samples were given accumulative thermal treatments in Ar and O₂ atmospheres separately. The first treatment was performed at 400 °C for 1 h, followed by a second treatment at 600 °C for 1 h in the same atmosphere.

3. Results and discussion

Secondary electron images of doped and undoped samples show a radial growth of tapered needle-shaped ZnO structures with diameter between 240 and 580 nm, and average length of 6 μm grouped in spherical clusters [Fig. 1(a) and (b)]. Particles of about 400 nm in diameter were also present in the In-doped samples as a by-product of the synthesis process, which could be easily separated from the needle-shaped ZnO crystals after a brief sonication in water [Fig. 1(c)]. Such nanoparticles are indium rich as has been previously reported [18].

CL images of the undoped sample revealed inhomogeneous CL intensity distribution along the length of the rod-like nanostructures [Fig. 2(a) and (b)] with brighter regions corresponding to a higher density of point defects, that act as radiative centers analogously to the observations made for CdSe needles [19]. On the other hand, CL images of In-doped samples showed a more homogeneous intensity distribution along the ZnO nanorods [Fig. 2(c)–(h)]. To correlate indium content with the luminescent properties we performed EDS mapping on the samples. Fig. 3 shows a CL image together

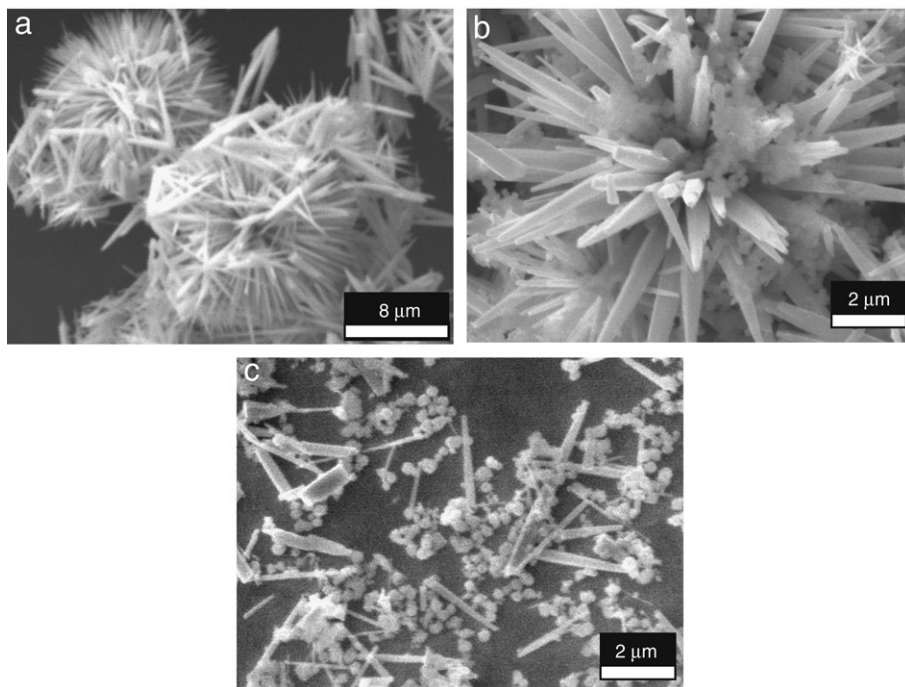


Fig. 1. Typical SEM images of ZnO nanostructures: (a) undoped, (b) 1.0%, and (c) 2.0% nominal indium doping (after a brief sonication in water).

with EDS maps of Zn, O and In for the 2% In doped sample. Similar images were recorded from the 1% doped sample. As expected, a homogeneous distribution of Zn and O in the sample was observed. However, very low luminescent emission was observed for the nanostructures with high In content [arrow in Fig. 3(e)], which is probably due to the formation of non-radiative centers produced by In incorporation into the ZnO nanostructures. Fig. 3 also shows a particle (labeled A) with almost no Zn or O content, but with a high concentration of indium and a faint CL emission. Formation of elemental indium has been reported in heavily In-doped ZnO films grown by spray pyrolysis using indium chloride as impurity source [20].

In Fig. 4(a) we present the CL spectra of the as-grown samples doped with different nominal percent of In, showing luminescence quenching that becomes more pronounced with increasing indium content. There appeared two emission bands centered at about 3.12 and 2.13 eV, which correspond to the near band edge emission and the well-known defect related yellow emission in ZnO, respectively. In this study, the CL spectra were acquired maintaining a constant electron-beam current density of about 1.8×10^{-3} nA/ μm^2 , which permits us to assign any change in the intensity ratio I_{UV}/I_{yell} to the variations due only to the electronic transitions in ZnO. Fig. 4(b)–(d) show CL spectra acquired at room temperature from the samples annealed in Ar atmosphere at 400 °C and 600 °C, and in oxygen atmosphere at 600 °C, respectively. The increase of I_{UV}/I_{yell} ratio in these samples with respect to the un-annealed samples [Fig. 4(a)] is due to a decrease in the density of point defects responsible for the yellow emission. Independent of the atmosphere used, a red shift of 180 meV at 400 °C [Fig. 4(b)] and 230 meV at 600 °C [Fig. 4(c) and (d)] for the defect-related emission band were observed for the annealed samples. On the other hand, the near band edge emission band shifts with the variation of In concentration. The observed variations in the position of the near band edge band [Fig. 4(b) and (c)] in indium incorporated annealed samples are possibly due to the variations in the density of shallow levels after annealing. The red shift of the near band edge emission band in the

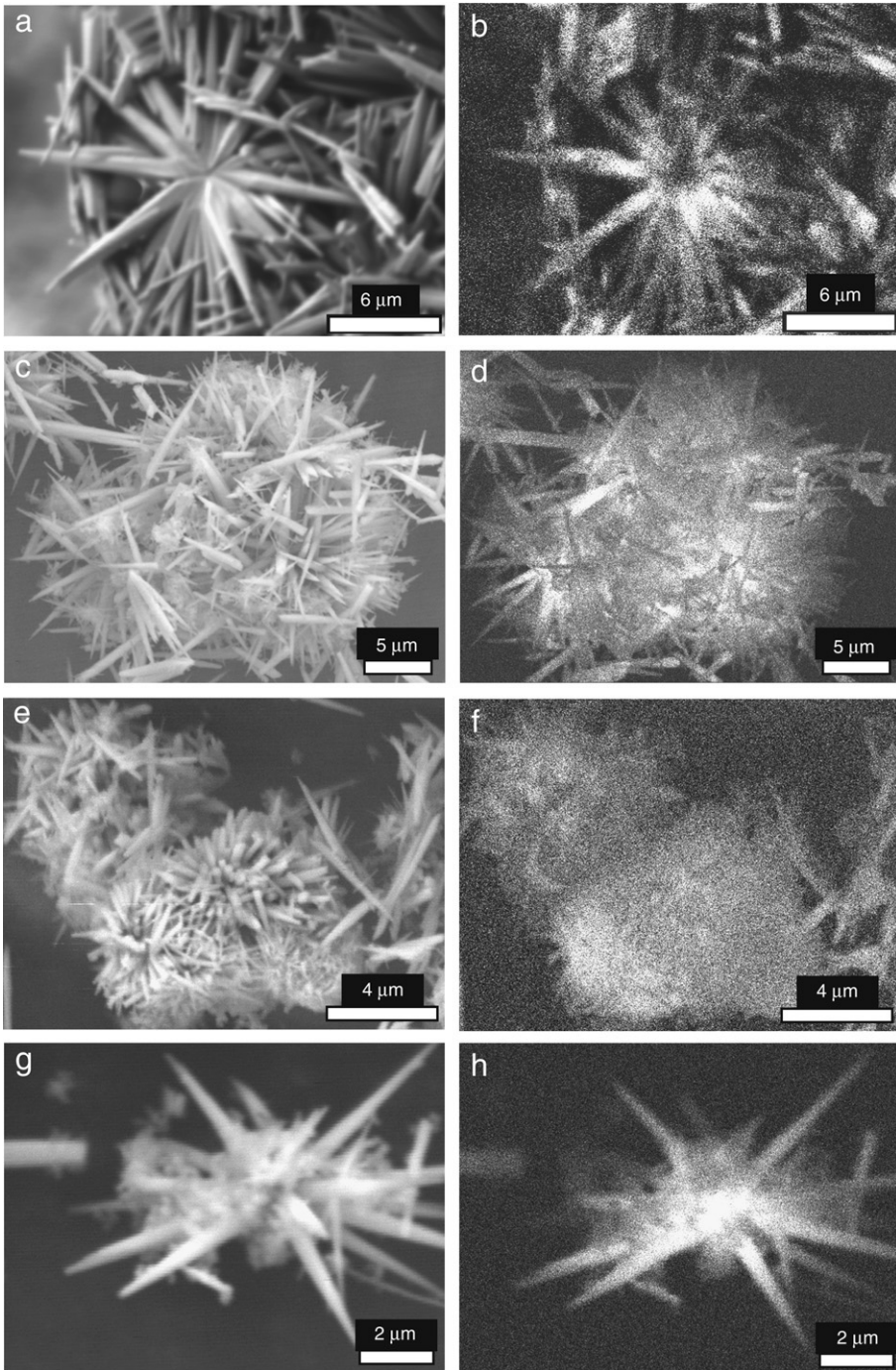


Fig. 2. SEM images and corresponding panchromatic CL images of undoped (a and b), nominal 0.5% (c and d), 1.0% (e and f), and 2.0% (g and h) indium doped samples.

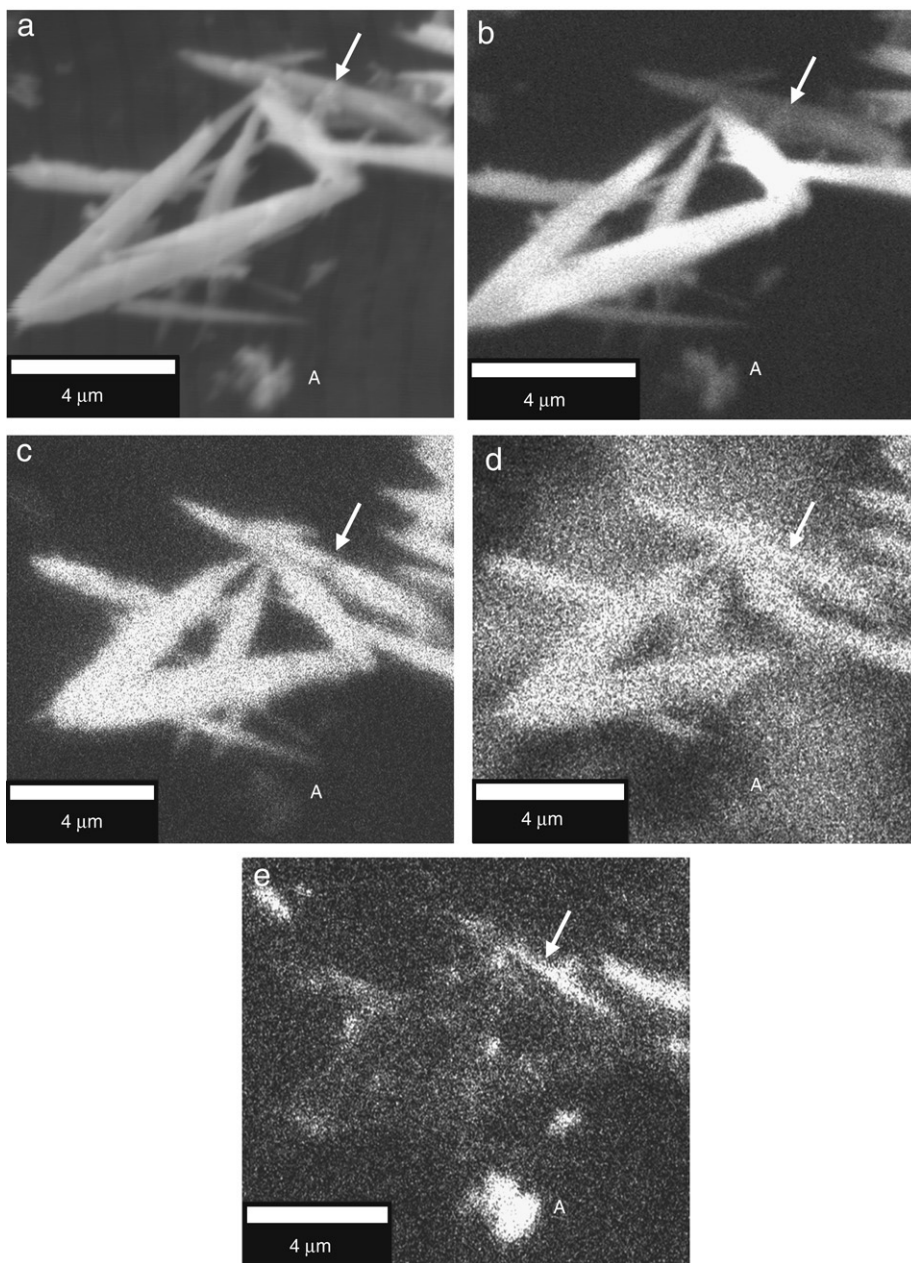


Fig. 3. (a) SEM image of the 2% nominal indium doped sample and (b) corresponding panchromatic CL image. EDS elemental mapping image of (c) zinc (K and L series), (d) oxygen (K series) and (e) indium (L series).

samples annealed in oxygen [Fig. 4(c)] atmosphere has been attributed previously to indium doping only [21,22].

Normalized CL spectra acquired at 100 K from the samples annealed in Ar and O₂ atmospheres are presented in Fig. 5. The defect-related band in these samples appeared at about 1.77 eV, with a clear shoulder at about 2.24 eV for the undoped and 1.0% In doped ones [Fig. 5(a) and (b)]. While the 2.24 eV

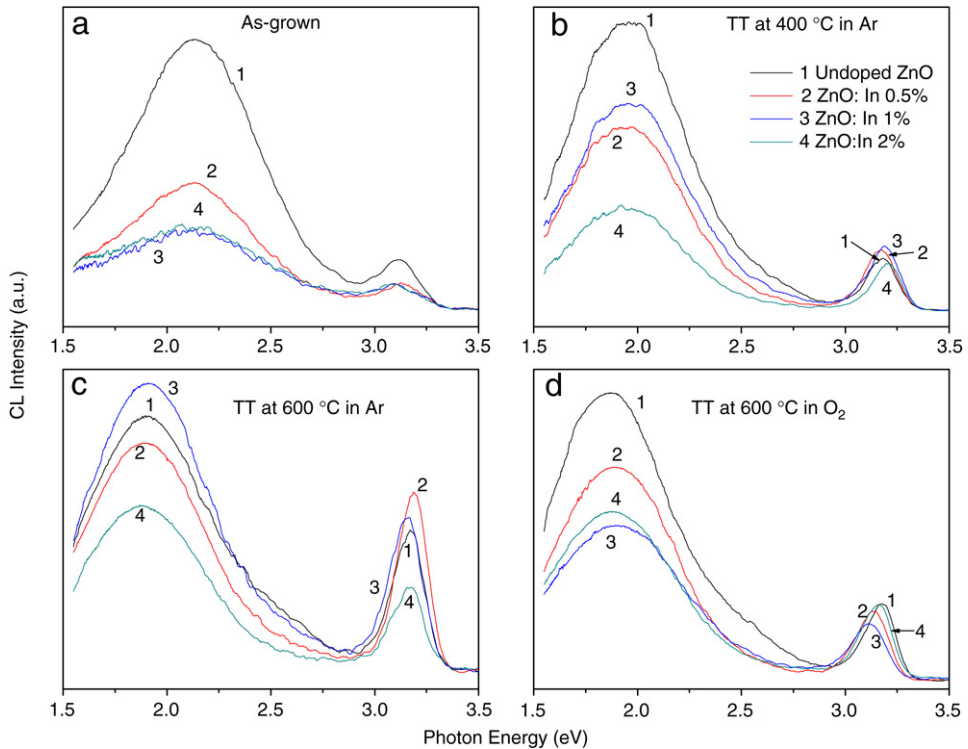


Fig. 4. (Color online) CL spectra acquired at room temperature for the ZnO nanostructures: (1) undoped, (2) 0.5%, (3) 1.0% and (4) 2.0% indium doped. (a) As-grown, (b) annealed at 400 °C in Ar atmosphere, (c) annealed at 600 °C in Ar atmosphere, and (d) annealed at 600 °C in O₂ atmosphere.

shoulder band is prominent for the 1% In doped sample, for 0.5% and 2% doped samples is practically non-existent. Fig. 5(c) shows a deconvoluted CL spectrum of the defect-related emission for the 1% In-doped sample, revealing two components centered at about 2.24 and 1.77 eV. The intensity ratio value of these two components $I_{2.24}/I_{1.77}$ varied with temperature, reaching a maximum value of 0.9 at 190 K [Fig. 5(d)].

Although the red shift of the defect-related emission after thermal annealing [Fig. 4(b)–(d)] is attributed to a reduction of radiative point defects in the samples, Fig. 5(a) and (b) reveal beside that this red shift is produced along with a decrease in the relative intensity of the 2.24 eV band. This last effect indicates that the defects responsible of this yellow band are reduced considerably after the thermal treatments, independent of atmosphere used. The formation of this 2.24 eV emission band has been attributed to electronic transitions between deep levels introduced by interstitial oxygen point defects [23]. Wu et al. have suggested that this emission is produced by the recombination of delocalized electrons close to the conduction band with deeply trapped holes in the O_i^- point defect levels [24]. Since a thermal treatment at 600 °C in oxygen atmosphere can result in oxygen incorporation into the ZnO lattice, an increase of O_i concentration is expected. We believe some other types of point defects are also responsible for the yellow emission. Radoi et al. [25] have reported a decrease of yellow emission intensity by aging ZnO sample and associated it to the annealing out or rearrangement of the defects responsible for this band by relaxation of stress. Thermal treatment in our samples, either in inert or in oxidative atmosphere results in the decrease of the yellow emission intensity, apparently with similar efficiency since in both the cases the $I_{2.24}/I_{1.77}$ ratio is similar [Fig. 5(a) and (b)]. Since the decrease of yellow band intensity occurs even for annealing at temperature as low as 400 °C [Fig. 4(b)], it is clear that the thermal treatments in Ar and O₂ produce efficient

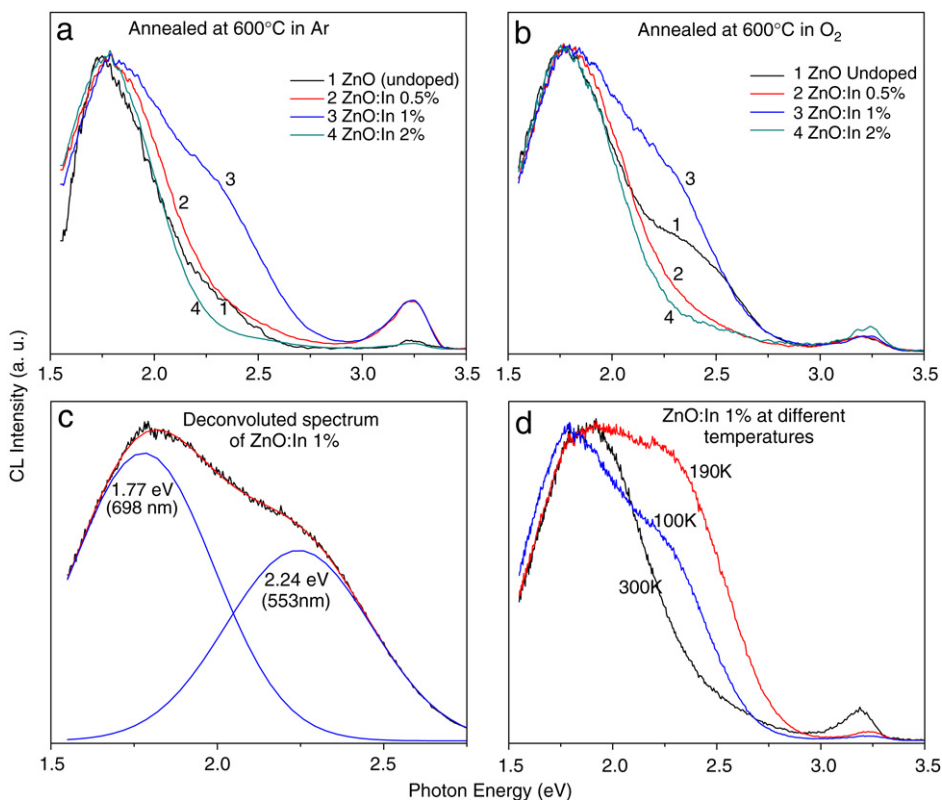


Fig. 5. (Color online) Low temperature (100 K) CL spectra of the samples with different % of In and annealed at 600 °C in (a) Ar and (b) O₂ atmospheres. (c) Deconvoluted defect-band showing two components centered at about 2.24 and 1.77 eV. (d) CL spectra acquired at different temperatures for the 1% In doped sample after annealing at 600 °C in Ar atmosphere.

annealing of yellow-related point defects in ZnO. Recently Erhart and Albe [26] have reported that Zn_i are the most mobile defects in ZnO and could be annealed out at temperatures as low as 90–130 K, in agreement with previous reports that reveal high diffusivity of this native defect [27,28]. We propose that the quenching of yellow emission in our annealed samples is due to the annealing of Zn_i defects. Finally, the red emission centered at 1.77 eV also revealed a decrease in their relative intensity after the thermal treatments [Fig. 4(b)–(d)]. Although this emission has been related to the presence of interstitial zinc [29,30], it has also been assigned to interstitial oxygen [31]. As can be seen from the Fig. 5(a) and (b), the annealing treatments eliminate the yellow emission related point defects more efficiently than the red emission related point defects, which apparently suggests that the interstitial oxygen atoms do not participate in the generation of the red-emission. Further studies are required to determinate the defects responsible for this emission.

4. Conclusions

Doped and undoped ZnO nanostructures with nominal 0.5, 1.0, and 2.0 mol% indium doping were grown by a low temperature hydrothermal technique. Quenching of CL emission occurs in the doped samples either due to the reduction of radiative point defects or by the formation of non-radiative defects. CL spectra of the as-grown samples reveal a broad defect emission band at about 2.12 eV apart from the near band edge emission at 3.2 eV. On annealing the samples at 400 °C and 600 °C either in Ar and O₂ atmospheres, the defect band shifts towards longer wavelength along with a reduction of intensity. The red shift of the broad defect-related band could be explained in terms of

the variation of relative intensities of its two component bands (at about 2.24 and 1.77 eV) that make up the broad band. On thermal annealing, the relative intensity of the yellow band centered at about 2.24 eV decreases due to the reduction of interstitial zinc in the samples.

Acknowledgements

This work was partially supported by grants from UC-MEXUS (No. CN-05-215), CONACyT (Grant # 47505 and 46269), PAPIIT-UNAM (Grant # IN107208) and VIEP-BUAP (Grant # 93/EXC/2008-1), Mexico. Technical helps of E. Flores and E. Aparicio are also acknowledged.

References

- [1] H. Dae-Kue, O. Min-Suk, L. Jae-Hong, C. Yong-Seok, P. Seong-Ju, *Appl. Phys. Lett.* 91 (2007) 121113.
- [2] H.S. Kim, F. Lugo, S.J. Pearton, D.P. Norton, Yu-Lin Wang, F. Ren, *Appl. Phys. Lett.* 92 (2008) 112108.
- [3] L. Liao, H.B. Lu, J.C. Li, C. Liu, D.J. Fu, *Appl. Phys. Lett.* 91 (2007) 173110.
- [4] J.Y. Son, S.J. Lim, J.H. Cho, W.K. Seong, Hyungjun Kim, *Appl. Phys. Lett.* 93 (2008) 053109.
- [5] L. Zi-Ling, D. Jian-Cheng, D. Jing-Jing, L. Fei-Fei, *Mater. Sci. Eng. B* 150 (2008) 99.
- [6] T. Chia-Lung, L. Yow-Jon, W. Ping-Hsun, C. Shu-You, L. Day-Shan, H. Jia-Huang, L. Chia-Jyi, S. Yu-Tai, C. Jie-Min, C. Hsing-Cheng, *J. Appl. Phys.* 101 (2007) 113713.
- [7] S.Y. Bae, C.W. Na, J.H. Kang, J. Part, *J. Phys. Chem. B* 109 (2005) 2526.
- [8] Y. Yang, J. Qi, Y. Zhang, Q. Liao, L. Tang, Z. Qin, *Appl. Phys. Lett.* 92 (2008) 183117.
- [9] F. Reuss, C. Kirchner, Th. Gruber, R. Kling, S. Maschek, W. Limmer, A. Waag, P. Ziemann, *J. Appl. Phys.* 95 (2004) 3385.
- [10] C. Diaz-Guerra, J. Piqueras, V. Popa, A. Cojocar, I.M. Tiginyanu, *Appl. Phys. Lett.* 86 (2005) 223103.
- [11] R.B.M. Cross, M.M. De Souza, E.M. Sankara-Narayanan, *Nanotechnology* 16 (2005) 2188.
- [12] L. Chun-Lee, H. Yuen-Yung, S. Wei-Fang, L. Ching-Fuh, *Appl. Phys. Lett.* 92 (2008) 261107.
- [13] H.J. Fan, R. Scholz, M. Zacharias, U. Gösele, F. Bertam, D. Forster, J. Christen, *Appl. Phys. Lett.* 86 (2005) 023113.
- [14] A. Urbietta, P. Fernández, Ch. Hardalov, J. Piqueras, T. Sekiguchi, *Mater. Sci. Eng. B* 91 (2002) 345.
- [15] K. Vanheusden, C.H. Seager, W.L. Warren, D.R. Tallant, J.A. Voigt, *Appl. Phys. Lett.* 68 (1996) 403.
- [16] A.F. Kohan, G. Ceder, D. Morgan, C.G. Van de Walle, *Phys. Rev. B* 61 (2000) 15019.
- [17] M. Herrera-Zaldivar, J. Valenzuela-Benavides, U. Pal, *Opt. Mater.* 27 (2005) 1276.
- [18] A. Escobedo Morales, M. Herrera Zaldivar, U. Pal, *Opt. Mater.* 29 (2006) 100.
- [19] A. Urbietta, P. Fernández, J. Piqueras, *Appl. Phys. Lett.* 85 (2004) 5968.
- [20] P.M. Ratheesh Kumar, C. Sudha Kartha, K.P. Vijayakumar, T. Abe, Y. Kashiwabe, F. Singh, D.K. Avasthi, *Semicond. Sci. Technol.* 20 (2005) 120.
- [21] H.J. Fan, B. Fuhrmann, R. Scholz, C. Himcinschi, A. Berger, H. Leipner, A. Dadgar, A. Krost, S. Christiansen, U. Gösele, M. Zacharias, *Nanotechnol.* 17 (2006) S231.
- [22] J. Jie, G. Wang, X. Han, Q. Yu, Y. Liao, G. Li, J.G. Hou, *Chem. Phys. Lett.* 387 (2004) 466.
- [23] S. Yamauchi, Y. Goto, T. Hariu, *J. Cryst. Growth* 260 (2004) 1.
- [24] K.L. Wu, G.G. Siu, C.L. Fu, H.C. Ong, *Appl. Phys. Lett.* 78 (2001) 2285.
- [25] R. Radoi, P. Fernández, J. Piqueras, M.S. Wiggins, *J. Solids, Nanotechnol.* 14 (2003) 794.
- [26] P. Erhart, K. Albe, *Appl. Phys. Lett.* 88 (2006) 201918.
- [27] A. Janotti, C.G. Van de Walle, *J. Cryst. Growth* 287 (2006) 58.
- [28] D.G. Thomas, *J. Phys. Chem. Solidus (USA)* 3 (1957) 229.
- [29] M. Gomi, N. Oorika, K. Ozaki, M. Koyano, *Japan. J. Appl. Phys.* 42 (2003) 481.
- [30] R.B. Cross, M.M. De Souza, E.M. Sankara-Narayanan, *Nanotechnol.* 16 (2005) 2188.
- [31] S.A. Studenikin, N. Golego, M. Cocivera, *J. Appl. Phys.* 84 (1998) 2287.